Struct Multidisc Optim (2013) 47:571–581
DOI 10.1007/s00158-013-0887-8

RESEARCH PAPER

Topology optimization for fluid–thermal interaction problems under constant input power

Tadayoshi Matsumori · Tsuguo Kondoh · Atsushi Kawamoto · Tsuyoshi Nomura

Received: 7 October 2011 / Revised: 30 November 2012 / Accepted: 6 January 2013 / Published online: 15 February 2013

Abstract This paper deals with density-based topology optimization considering fluid and thermal interactions, in which the Navier–Stokes and heat transport equations are coupled. We particularly focus on designing heat exchangers. In the engineering context, heat exchangers are designed while considering a certain amount of input power. Therefore it is important to maximize the performance of a heat exchanger under a constant input power. In this paper we propose a way to control the input power by introducing an extra integral equation. To be more precise, in the fluid analysis, the inlet pressure is determined by solving the extra integral equation together with the Navier–Stokes equation. By doing this we can keep the inlet power constant even when the flow channels are changed in the optimization process. Consequently, the system of equations of the fluid field takes an integrodifferential form. On the other hand, in the heat transport analysis, a single governing equation is defined for simultaneously modeling both the solid and fluid parts. The design variable is a fluid fraction whose distribution represents the topology of the solid and fluid domains. When designing heat exchangers, two different heat conditions are considered in the formulation of the optimization problems, namely temperature-dependent and temperature-independent heat sources. Through the numerical examples for designing flow channels in a heat exchanger, it is shown that distinct topologies can be obtained according to the input power and the heat source conditions.

T. Matsumori (✉) · T. Kondoh · A. Kawamoto
Toyota Central R&D Labs., Inc., Nagakute Aichi 480-1192, Japan
e-mail: matsumori@mosk.tytlabs.co.jp

T. Nomura
Toyota Research Institute of North America,
1555 Woodridge Avenue, Ann Arbor, MI, 48105, USA

Keywords Topology optimization · Fluid–thermal interaction · Heat transfer

1 Introduction

Topology optimization was proposed in 1988 by Bendsøe and Kikuchi (1988). For the last two decades several optimization methods for topology optimization have been developed: e.g., the homogenization method (Bendsøe and Kikuchi 1988), the Solid Isotropic Material with Penalization (SIMP) method (Bendsøe 1989; Rozvany et al. 1992), and the level set method (Wang et al. 2003; Allaire et al. 2004). These methods have been successfully applied to many problems, not only structural but also fluid or thermal optimization problems.

As regards thermal field optimization problems, the heat conduction problems governed by the Poisson equation have been well studied because of their relatively simple constitutive equations. Bendsøe and Sigmund (2003) and Gersborg-Hansen et al. (2006) formulated a heat conduction problem of minimum resistance using the SIMP method. Li et al. (2004) applied the evolutionary structural optimization method (Rozvany 2009) to the heat conduction problems. Bruns proposed the SINH method (Bruns 2005) and applied it to convection dominated heat transfer problems (Bruns 2007). Iga et al. (2009) applied the homogenization method to the structural design under thermal load considering the heat conduction and convection.

On the other hand, in the area of flow field optimization, the classical research done by Pironneau (1973) analytically presented the optimal shape in the Stokes flow. As for numerical shape optimization for fluid dynamics problems, a comprehensive summary can be found in Mohammadi and Pironneau (2009). We also refer to Katamine et al.

(2005) regarding the minimization of the total dissipation energy using the traction method (Azegami 1994; Azegami and Takeuchi 2006). For topology optimization, Borrvall and Petersson (2003) presented a density-based approach to minimizing the power dissipated in the Stokes flow. The method has been expanded to cover the incompressible Navier–Stokes equations in a steady state (Gersborg-Hansen et al. 2005; Olesen et al. 2006; Pingen et al. 2007; Aage et al. 2008). Kondoh et al. (2012) proposed parameter settings for stabilizing the optimization processes and various types of objective functions for minimizing the drag force and maximizing the lift force.

Recently, topology optimization has also been applied to fluid–thermal interaction problems, i.e., coupled problems of the Navier–Stokes equation and advection-diffusion equations. Okkels and Bruus (2007) applied topology optimization to a microfluidic reactor design problem modeled by advection-diffusion-reaction equations with a constant pressure drop between the inlet and the outlet as the boundary condition, in which the distribution of immobilized cultures within a nutrition flow was optimized in order to maximize the reaction rate. Dede (2009) extended the method to the fluid–thermal interaction problem for minimizing the weighted sum of the mean temperature and dissipation energy under a given inlet velocity, and applied the method to a hierarchical microchannel system design (Dede 2011). Yoon (2010) proposed a similar method for designing a heat dissipating structure under a constant mass flow; all the material properties were interpolated based on the SIMP method, and the structure was designed so as to minimize the thermal compliance. The method was extended to the design procedure of an electro-thermal-compliant actuator device (Yoon 2012). These previous studies utilized the finite element method, while Pingen and Meyer (2009) applied the lattice Boltzmann method to a topology optimization method for heat transfer applications. They designed flow channels by minimizing the average temperature under a constraint of total pressure loss.

In this paper, we will focus on designing heat exchangers. Generally, heat exchangers are designed to maximize performance given a certain amount of input power. However, the condition of constant input power cannot be realized using simple inlet boundary conditions as treated in the previous studies for fluid field and fluid–thermal interaction problems. Therefore, we propose a way to keep the input power constant within the optimization process for maximizing heat transfer. Specifically, we solve an extra integral equation to determine the inlet pressure, and then pass the results to the boundary condition of the Navier–Stokes equation in the fluid analysis. By doing this, the inlet power can be kept constant when the flow channels in the heat exchanger are redesigned in the optimization process. Consequently, we construct an integrodifferential form for the system of equations of the fluid field. For the Navier–Stokes equation, based on the Borrvall's approach (Borrvall and Petersson 2003), it is assumed that the fluid flow in the idealized porous medium is parameterized with a fluid fraction which is utilized as the design variable. The distribution of the fluid fraction represents the topology of the solid and fluid domains. For the heat transport analysis, there are two governing equations for the solid and fluid domains. To simultaneously model both the solid and fluid domains, the two equations are unified into a single equation using the design variables. The optimization problem is then formulated for the maximization of heat transfer with respect to two types of heat sources: temperature-dependent and temperature-independent heat sources. In this formulation, the constant input power condition does not appear as an explicit equality constraint; the condition is, in a sense, hidden behind the optimization process. The constant input power condition is, instead, ensured by solving the additional integral equation together with the Navier–Stokes equation and the transport equation. For application examples, we design the flow channels of two-dimensional heat exchangers with different power and heat source conditions.

This paper is organized as follows. In Section 2, we introduce the modified governing equations of the fluid and thermal fields for topology optimization, and formulate the optimization problem for the maximization of heat transfer. Section 3 shows the algorithm of the topology optimization. In Sections 4 and 5, we present and discuss numerical examples for designing the flow channels in two-dimensional heat exchangers. Finally Section 6 concludes the current research.

2 Formulation for topology optimization of fluid–thermal interaction problems

In this paper we are going to design the flow channels of heat exchangers that maximizes heat transfer. To this end we first describe the design representation for topology optimization, then present the governing equations for fluid–thermal interaction problems which are modified for topology optimization, and finally formulate relevant optimization problems for the maximization of heat transfer.

2.1 Design representation

The problem setting is shown in Fig. 1 where the geometry of the model and all the related boundary conditions are depicted. The design domain D is the 3×3 square area.

Following the research by Borrvall and Petersson (2003), we introduce a fluid fraction, γ, as the design variable. The fluid fraction, γ, varies continuously from zero to one: $\gamma = 0$ stands for solid and $\gamma = 1$ for fluid. In this setting the

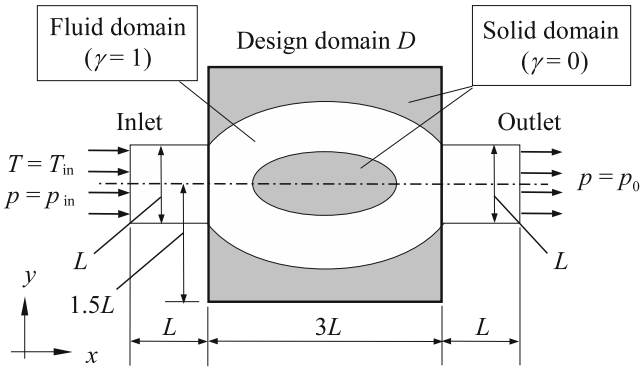

Fig. 1 Problem setting for designing a heat exchanger with one inlet and one outlet

fluid flow in the design domain is modeled with an idealized porous media. The local porosity indicated by γ also means a local non-dimensional fluid density. Note that this setting is essentially the same as the density method in structural optimization.

2.2 Fluid field modeling

The governing equations of the incompressible steady fluid flow are given for the velocity, $\mathbf{u}$, and the pressure, p, with the density, ρ, and the viscosity, μ, as

$$\nabla \cdot \mathbf{u} = 0, \tag{1}$$

$$\rho\,(\mathbf{u} \cdot \nabla)\,\mathbf{u} = -\nabla p + \mu \nabla^2 \mathbf{u} + F, \tag{2}$$

where F is a body force caused by the solid objects in the flow, namely the porous media. Assuming the resistive force due to the porous media in the flow is proportional to the fluid velocity, $\mathbf{u}$, the body force is modeled as

$$F = -\alpha \mathbf{u}, \tag{3}$$

where $\alpha(\mathbf{x})$ is the inverse permeability of the porous media at position $\mathbf{x}$ (Borrvall and Petersson 2003).

In the following numerical examples we will solve (1) and (2) under a constant input power, P. In order to ensure the constant input power, we introduce the following integral equation with respect to the inlet pressure, p_{in}:

$$\int_{\Gamma_{\text{in}}} p_{\text{in}}\, u \, \mathrm{d}\Gamma = P. \tag{4}$$

The system is augmented by including p_{in} as a variable. Then p_{in} is passed to the inlet boundary condition of (2). Consequently, for the fluid analysis, we obtain the system of *integrodifferential equations* (1), (2), and (4).

Equations (1) and (2) can be transformed into a dimensionless form using dimensionless variables:

$$\mathbf{x}^* = \frac{\mathbf{x}}{L},\ \nabla^* = L\nabla,\ \mathbf{u}^* = \frac{\mathbf{u}}{U},$$

$$p^* = \frac{p - p_0}{\rho U^2},\ \alpha^* = \frac{L\alpha}{\rho U^2}. \tag{5}$$

Here, L and U are the characteristic length and velocity, and p_0 is the outlet pressure. The dimensionless forms of (1) and (2) together with the body force expression (3) are written as

$$\nabla^* \cdot \mathbf{u}^* = 0, \tag{6}$$

$$\left(\mathbf{u}^* \cdot \nabla^*\right)\mathbf{u}^* = -\nabla^* p^* + \frac{1}{\mathrm{Re}}\nabla^{*2}\mathbf{u}^* - \alpha^*\mathbf{u}^*, \tag{7}$$

where $\mathrm{Re} \equiv \rho U L/\mu$ is the Reynolds number. $\alpha^*(\mathbf{x}^*)$ is the dimensionless inverse permeability which is given by

$$\alpha^* = \alpha^*_{\max}\alpha'(\gamma), \tag{8}$$

$$\alpha'(\gamma) = \frac{q(1-\gamma)}{q+\gamma}, \tag{9}$$

where q is a positive parameter used for tuning the function shape of $\alpha'(\gamma)$.

It is desirable that $\alpha^*_{\max}$ is always large enough to keep the significance of the body force term, $\alpha^*\mathbf{u}^*$, higher than the others regardless of the Reynolds number. This ensures that the velocity in the solid domain ($\gamma = 0$) vanishes. Hence $\alpha^*_{\max}$ is defined, depending on the Reynolds number, as follows (Kondoh et al. 2012):

$$\alpha^*_{\max} = \left(1 + \frac{1}{\mathrm{Re}}\right)\frac{1}{\mathrm{Da}}, \tag{10}$$

where Da is the Darcy number which takes on a small positive value. In the current study, q and Da are set to 10^{-2} and 10^{-4}, respectively.

As regards Re, the inlet velocity is normally used as the characteristic velocity, U. However the inlet velocity may alter in the fluid analysis under the condition of constant input power because the flow channels in the heat exchanger are changed during the optimization process. In other words, the Re based on the inlet velocity depends on the design of the flow channels. Therefore, in this paper, to obtain the optimized results under the constant input power, P, we determine the characteristic velocity U based on the power P:

$$P = \rho U^3 L^2. \tag{11}$$

Thus, the dimensionless version of (4) is given by

$$\int_{\Gamma_{\text{in}}} p^*_{\text{in}}\, u^* \, \mathrm{d}\Gamma = 1. \tag{12}$$

With this condition, the input power, P, becomes proportional to Re^3, as

$$P = \frac{\mu^3}{\rho^2 L}\mathrm{Re}^3. \tag{13}$$

In this paper, we solve the differential equations (6) and (7), and the integral equation (12), simultaneously.

2.3 Thermal field modeling

There are different governing equations for the thermal field in the fluid and solid domains. When the heat source is only placed in the solid domain, with the specific heat of the fluid, c, and the thermal conductivities of the fluid and solid parts, k_f and k_s, the governing equations can be expressed for the temperature, T, as

$$\rho c\,(\mathbf{u}\cdot\nabla)\,T = k_\mathrm{f}\nabla^2 T, \qquad \text{(in fluid domains)} \quad (14)$$

$$0 = k_\mathrm{s}\nabla^2 T + Q, \qquad \text{(in solid domains)} \quad (15)$$

where Q is the heat generation per unit time and volume.

In topology optimization, the distribution of the fluid and the solid domains can only be determined after the optimization. Therefore, one cannot know a priori which equation should be adopted at each point. To solve this issue using the fluid fraction γ, the two equations, (14) and (15), are unified into the following single equation which is applicable to both the fluid and solid domains:

$$\gamma\frac{1}{a}\,(\mathbf{u}\cdot\nabla)\,T = \{(1-\gamma)K+\gamma\}\,\nabla^2 T + (1-\gamma)\frac{Q}{k_\mathrm{f}}, \quad (16)$$

where $a \equiv k_\mathrm{f}/\rho c$ is the thermal diffusivity of the fluid and $K \equiv k_\mathrm{s}/k_\mathrm{f}$ is the ratio of the solid and fluid thermal conductivities. Equation (16) represents a general mapping between the fluid and solid domains. In this work, the equation is further simplified by setting $K = 1$.

With respect to the heat source, Q, we consider two cases. In the first case the heat source is dependent on the local temperature, while in the second case the heat source is independent. The former assumes that the heat transfer ratio is given at the interface, and the latter that uniform heat flux is set by the solid regions. Let us rewrite (16) in a non-dimensional form with the dimensionless parameter, Pr (called the Prandtl number), and the dimensionless temperature, T^*, in addition to $\mathbf{u}^*$, p^* as defined by (5):

$$\mathrm{Pr} = \frac{\mu}{\rho a},\quad T^* = \frac{T - T_\mathrm{in}}{T_\mathrm{Q} - T_\mathrm{in}}, \quad (17)$$

where T_in is the inlet temperature, and T_Q is another reference temperature. The definition of T_Q depends on two cases explained in the following subsections.

2.3.1 Temperature-dependent heat source

We assume an idealized heat source with temperature, T_Q, which can supply heat proportional to the difference between T_Q and the local temperature, T, in the solid domain:

$$Q = h\left(T_\mathrm{Q} - T\right), \quad (18)$$

where h is the coefficient that controls the heat generation according to the temperature difference. Substituting (18) into (16) with the expressions (5) and (17), we finally obtain the following dimensionless equation:

$$\gamma\mathrm{RePr}\left(\mathbf{u}^*\cdot\nabla^*\right)T^* = \{(1-\gamma)K+\gamma\}\,\nabla^{*2}T^* + (1-\gamma)\beta(1-T^*), \quad (19)$$

where β is the dimensionless heat generation coefficient defined as

$$\beta = \frac{hL^2}{k_\mathrm{f}}. \quad (20)$$

2.3.2 Temperature-independent heat source

Assuming that the total heat generation is controlled to be constant as H, and that the heat is uniformly distributed in the solid domain, the heat source term is expressed, with the volume of the solid domain, V, as

$$Q = \frac{H}{V},\ \text{where } V \equiv \int_D (1-\gamma)\mathrm{d}\Omega. \quad (21)$$

The reference temperature, T_Q, in this case is defined based on H by the following equation:

$$H = k_\mathrm{f}(T_\mathrm{Q} - T_\mathrm{in})L. \quad (22)$$

Using (22), (16) is rewritten in the following dimensionless form:

$$\gamma\mathrm{RePr}\left(\mathbf{u}^*\cdot\nabla^*\right)T^* = \{(1-\gamma)K+\gamma\}\,\nabla^{*2}T^* + \frac{(1-\gamma)}{V^*}, \quad (23)$$

where $V^* \equiv V/L^3$ is the dimensionless volume of the solid domain.

For brevity we will henceforth drop the asterisk of the dimensionless variables, $\mathbf{u}^*$, p^*, T^*, and V^*, and simply denote them as $\mathbf{u}$, p, T and V, respectively.

2.4 Optimization problems

In this section, under the two different heat conditions expressed by (18) and (21), we will respectively formulate two relevant optimization problems for the maximization of heat transfer. Note that these optimization problems implicitly include the equality constraint for the power which is kept constant by solving the integral equation (12).

2.4.1 Maximization of heat transfer with a temperature-dependent heat source

When the heat source is given by (18), we evaluate the heat transfer performance in terms of the total amount of

heat generation, Q, in the design domain. The optimization problem is formulated without any constraint as

Problem 1

$$\underset{\gamma\in[0,1]}{\text{maximize}}\ f := \int_D (1-\gamma)\beta(1-T)\,\mathrm{d}\Omega. \tag{24}$$

Please note that the objective function implicitly depends on the design variable, γ, through the temperature field, T, that is determined after solving the multi-physics problem defined by the system of *integrodifferential equations* (6), (7), (12), and (19). Since the forward analysis problem is hidden behind the optimization problem, this type of formulation is called a nested formulation.

2.4.2 Maximization of heat transfer with a temperature-independent heat source

Assuming that the heat source in the solid domain is given by (21), the mean temperature in the solid domain can be used as the performance measure for the target heat exchanger. Introducing a total volume constraint with V, the optimization problem can be formulated as

Problem 2

$$\begin{aligned}&\underset{\gamma\in[0,1]}{\text{minimize}}\ f := \frac{1}{V}\int_D (1-\gamma)T\,\mathrm{d}\Omega\\ &\text{subject to}\ g := V - \int_D (1-\gamma)\,\mathrm{d}\Omega = 0,\end{aligned} \tag{25}$$

where the temperature field in the objective function is evaluated through the nested analysis of the thermofluid system defined by the system of *integrodifferential equations* (6), (7), (12), and (23).

3 Algorithm for topology optimization

Problems 1 and 2 are solved by iterative calculations. The main flow of the algorithm for the topology optimization is described in Table 1.

Table 1 Algorithm of topology optimization for the maximization of heat transfer

Step 0	Set all the constants: Re, Pr, and β or V.
Step 1	Set initial values for γ.
Step 2	Solve the forward problems (6), (7), (12), (19) or (23).
Step 3	Calculate the sensitivities $\mathrm{d}f/\mathrm{d}\gamma$, $\mathrm{d}g/\mathrm{d}\gamma$.
Step 4	Evaluate the optimality condition. If a stopping criterion is met, terminate the calculation.
Step 5	Update the design variables γ and return to Step 2.

The forward problems and the optimization processes are implemented using COMSOL Multiphysics (COMSOL Multiphysics 2008). As for the optimization method, a sequential quadratic optimization solver SNOPT (Gill et al. 2007), built into the software package, is used. In SNOPT, the complementarity gap, which indicates how well the KKT condition is fulfilled, is used for a stopping criterion. The optimization process is terminated when the gap becomes less than the given small positive value called optimality tolerance (Kawamoto et al. 2011). Note that the temperature, T, is an implicit function of the design variable, γ, and that the derivative of the objective function with respect to the design variable, $\mathrm{d}f/\mathrm{d}\gamma$, is not directly available. For the implicit differentiation, a standard adjoint variable method is applied; for details, please refer to Bendsøe and Sigmund (2003) and Olesen et al. (2006).

4 Numerical examples 1

We are going to design flow channels for maximizing heat transfer in the two dimensional model depicted in Fig. 1 based on the algorithm listed in Table 1. Since the model is symmetric across the horizontal centerline, the upper half model is discretized by 4-node quadratic elements in the forward analysis. The total number of elements reaches 2,200. We present the numerical results of Problems 1 and 2 in the following subsections.

We will solve the two problems, where the heat source is expressed by (18) and (21) respectively, at different Reynolds numbers, Re, and the parameter β or V. The Prandtl number, Pr, for (19) and (23) is set to 6.78 assuming the working fluid is water. As boundary conditions for the governing equations (7) and (19) or (23), a no-slip condition is given on the walls, the inlet temperature is set to 0, and the thermal insulation condition is applied to all the other boundaries.

4.1 Results for temperature-dependent heat source (Problem 1)

Prior to the optimization, the initial value of the fluid fraction γ is set to 1 in which the objective function takes the worst value. Figure 2 provides three snapshots of the optimization process at Re $= 100$, $\beta = 100$, showing the fluid fraction, γ, the flow velocity, $\mathbf{u}$, the pressure, p, and the temperature, T, at iteration steps 8, 16, and 90, respectively. Figure 3 shows the optimization histories of the objective function and the relative complementarity gap. The optimization converged after 90 steps by fulfilling the stopping criterion where the complementarity gap is less than 10^{-5}. Note that after 16 iterations the distinct topology of the cooling channel can be observed. In the final design, gray

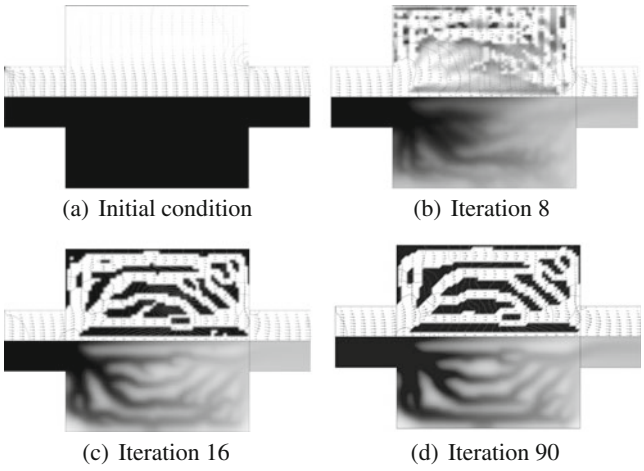

(a) Initial condition (b) Iteration 8

(c) Iteration 16 (d) Iteration 90

Fig. 2 Optimization process of the fluid fraction, γ, with Re $= 100$ and $\beta = 100$: (*upper half*) gray scale images of the fluid fraction, γ, vector plots of the flow velocity, u, and contour lines of the pressure, p; (*lower half*) distributions of the temperature, T

areas and isolated pools disappear. The fluid temperature increases gradually from the inlet to the outlet, and becomes uniform around the outlet.

Figure 4 shows a representative collection of the optimized flow channels at different combinations of the two parameters: the Reynolds number, Re, is set to {10, 20, 50, 100} and the heat generation coefficient, β, is set to {10, 20, 50, 100}. This figure illustrates the fluid fraction, γ, in gray scale with the flow represented by arrows and the temperature field by contours. The objective function value and the total number of iterations of the optimization process are described together with the figures. The optimized flow channels at high Re become narrower and more branched. The objective function values increase with Re under the same β, namely the same heat condition that is given column-wise. In this problem setting the input power, P, increases with Re ($P \propto \mathrm{Re}^3$) when the fluid properties,

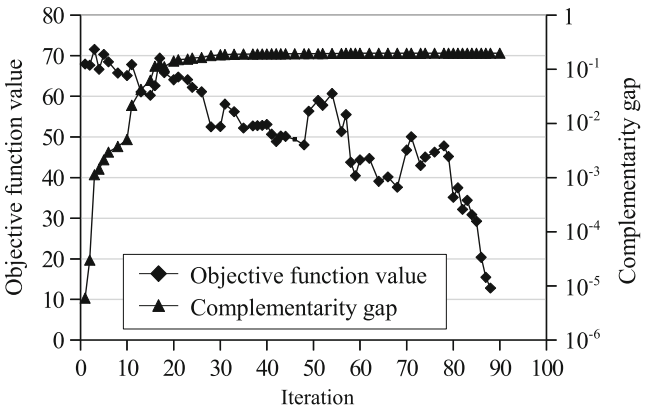

Fig. 3 Optimization histories of the objective function value and the relative complementarity gap for Re $= 100$ and $\beta = 100$

ρ and μ, and the characteristic length, L, are kept constant. The large power allows more complicated flow channels, and eventually elongates the heat transfer interface. This leads to the high performance of the heat exchanger. On the other hand, the same Re is applied row-wise. The solid islands become smaller with the increase of β. From the results, each combination of Re and β gives a different type of flow channel topology for maximizing the heat transfer.

To understand mesh dependency, we solve the same problem with a mesh that is twice as fine (8,800 elements). Figure 5 shows the two distinctive numerical results at Re $=$ {10, 100} and $\beta = 100$. The optimized flow channels with the finer mesh are different from those with the coarse mesh shown in Fig. 4. Interestingly, the objective function value at Re $= 100$ with the finer mesh is higher than that with the coarse mesh. In the cases of Re $= 100$ with a different β (not shown here), similar results are observed with the finer mesh. In minimum compliance problems, for instance, without using any filtering technique and with finer meshes, one may obtain mesh dependent optimized results with smaller (better) objective function values. In the current problem setting, this trend is also seen in the cases of low Re. On the other hand, with the increase of Re, it is anticipated that the advection term becomes more and more significant in the Navier–Stokes equation, and that the optimization problem becomes more and more non-convex with more local minima. Since SNOPT is a gradient-based optimization method, the local optimality is only guaranteed within the mesh resolution.

4.2 Results for temperature-independent heat source (Problem 2)

For Problem 2 the design variables are uniformly initialized with one of the feasible values in the design domain. This optimization problem is solved with different pairs of parameters: the Reynolds number, Re $=$ {10, 20, 50, 100}, and the total volume of the solid domain, $V = \{0.2, 0.3, 0.4, 0.5\}$. Figure 6 provides three snapshots of the optimization process at Re $= 100$ and $V = 0.5$, showing the fluid fraction, γ, the flow velocity, $\mathbf{u}$, the pressure, p, and the temperature, T, at iteration steps 10, 20, and 119, respectively. Figure 7 shows the optimization histories of the objective function and the relative complementarity gap. The optimization converged after 119 steps by fulfilling the stopping criterion where the complementarity gap is less than 10^{-6}.

Figure 8 illustrates a representative collection of optimized flow channels at different combinations of Re and V. The smaller V and the higher Re become, the smaller islands and the narrower flow channels that appear. In this case, the objective function value represents the mean temperature in the solid regions. As Re increases under the same

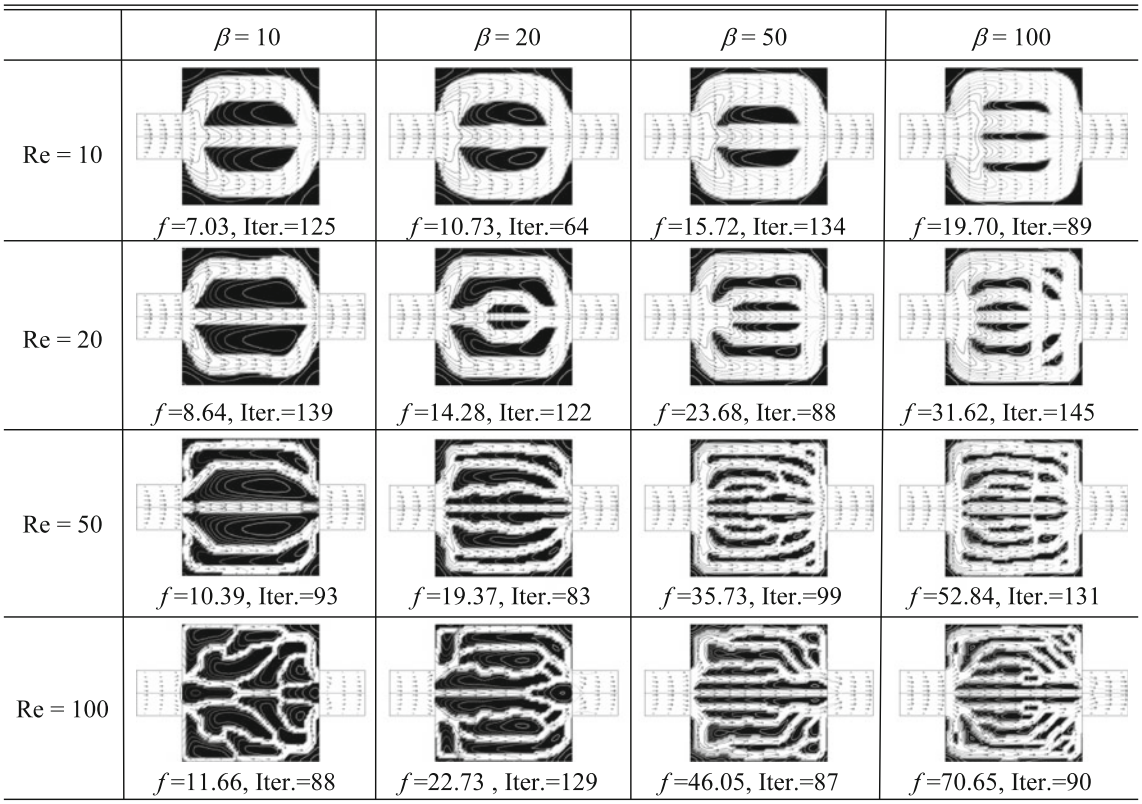

Fig. 4 Representative collection of optimized heat exchangers of Problem 1, which shows a fluid fraction γ in gray scale with arrows representation of the flow and contour lines of the temperature. In this problem setting, the input power, P, is eventually kept constant row-wise because P is proportional to Re^3

V, the objective function values decrease. That is, the performance of the optimized heat exchanger is improved with the increase of Re.

Comparing the optimized flow channels in Problems 1 and 2, one may notice that 13 out of the 16 results in Problem 1 have a flow channel directly connected from the inlet

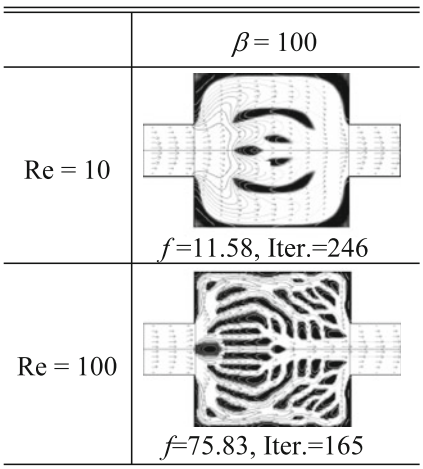

Fig. 5 Optimized heat exchangers of Problem 1 using a fine mesh (8,800 elements) at $\mathrm{Re} = \{10, 100\}$, and $\beta = 100$. The fluid fraction, γ, is shown in gray scale with the arrows representing the flow and the contour lines of the temperature

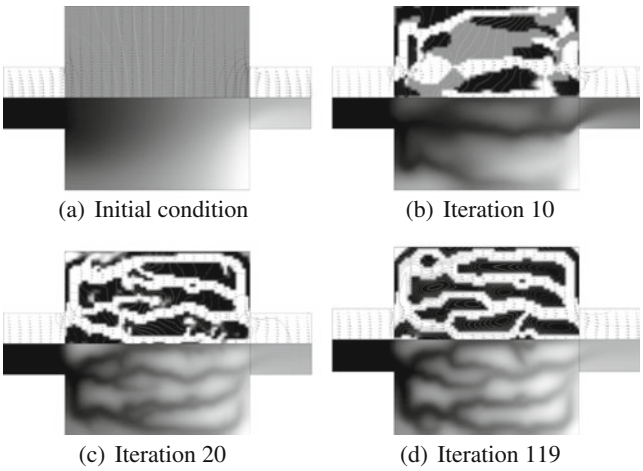

Fig. 6 Optimization process of the fluid fraction, γ, with $\mathrm{Re} = 100$ and $V = 0.5$: (*upper half*) gray scale images of the fluid fraction, γ, vector plots of the flow velocity, $\mathbf{u}$, and contour lines of the pressure, p; (*lower half*) distributions of the temperature, T

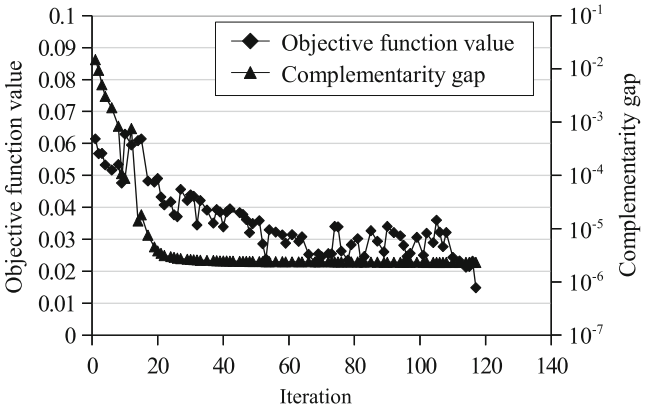

Fig. 7 Optimization histories of the objective function value and of the relative complementarity gap in the case where Re = 100 and $V = 0.5$

to the outlet right on the centerline, while none of the results in Problem 2 have a directly connected channel on the centerline. In Problem 1 all the design variables for the fluid fraction are initially set to 1, meaning that the whole domain is filled with fluid. Looking at the history of the design variables in Fig. 2, the central channel is formed at a relatively early stage of the optimization. It might be hard for a gradient-based optimization method like SNOPT to change the shortest central channel once formed in the optimization. However more careful studies have yet to be done for explaining why this does not occur in Problem 2.

Another issue is that the current model for the topology optimization allows a continuous pressure distribution in the solid regions due to the expression in (7). This is the critical difference from the model used in a flow analysis with a body-fitted configuration, in which the pressure is not defined in the solid regions. The current formulation may lead to errors in the numerical results as pointed out in Kreissl et al. (2011). To see the influence of the formulation on the numerical simulations, we prepared the body-fitted configuration which corresponds to the optimized design at Re = 100 and $V = 0.2$, as shown in Fig. 8. Figure 9 shows the results of the fluid–thermal coupling analysis with the body-fitted configuration compared with the optimized results. Note that the body-fitted configuration is discretized by 47,601 triangular elements, which is a much finer mesh than in the original configuration. The pressure distributions look similar and the difference between the objective function values is small. It seems fair to say that the errors caused by the expression of the solid region are at a tolerable level within the numerical simulations treated in this paper.

	$V = 0.5$	$V = 0.4$	$V = 0.3$	$V = 0.2$
Re = 10	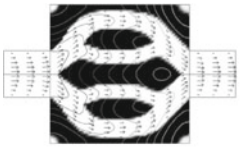 f=0.22, Iter.=274	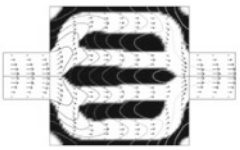 f=0.15, Iter.=259	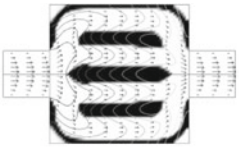 f=0.096, Iter.=121	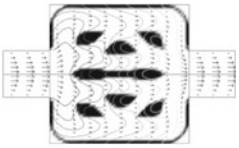 f=0.058, Iter.=114
Re = 20	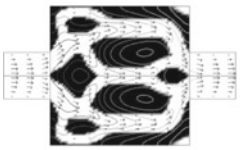 f=0.11, Iter.=420	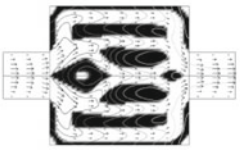 f=0.072, Iter.=132	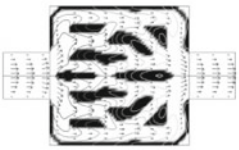 f=0.045, Iter.=159	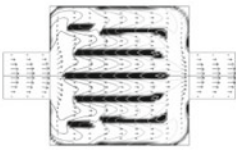 f=0.026, Iter.=75
Re = 50	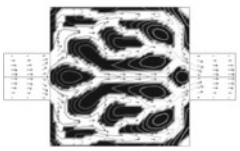 f=0.043, Iter.=76	 f=0.027, Iter.=301	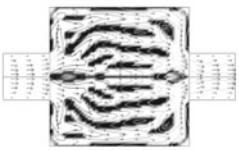 f =0.018, Iter.=280	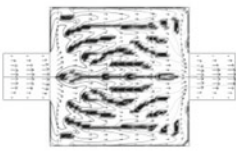 f=0.0098, Iter.=74
Re = 100	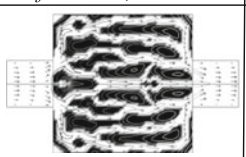 f=0.023, Iter.=119	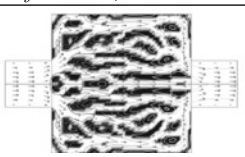 f=0.015, Iter.=59	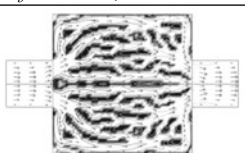 f=0.0089, Iter.=80	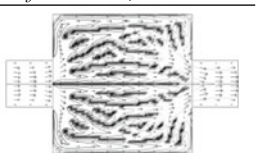 f=0.0049, Iter.=52

Fig. 8 Representative collection of optimized heat exchangers of Problem 2, which shows a fluid fraction γ in gray scale with arrows representation of the flow and contour lines of the temperature. In this problem setting, the input power, P, is eventually kept constant row-wise because P is proportional to Re^3

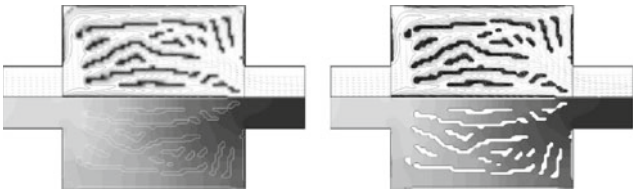

(a) Optimized design: f=0.0049 (b) Body-fitted configuration: f=0.0052

Fig. 9 Comparison of numerical simulations between the optimized design and the corresponding body-fitted configuration: (*upper half*) gray scale images of flow channels, vector plots of the flow velocity, **u**, and contour lines of the temperature, T; (*lower half*) distributions of the pressure, p

5 Numerical examples 2

In the second numerical example, we apply the proposed method to the problem of designing a heat exchanger with one inlet and two outlets, as shown in Fig. 10. A similar problem setting was also treated in Dede (2009), but note that the formulation of Dede (2009), which minimizes the dissipation energy and mean temperature simultaneously, is slightly different from that of the current paper. We solve Problems 1 and 2 using this model. For the two problems the design variables are uniformly initialized to 0.5 in the design domain.

Figure 11 provides three snapshots of the optimization process at Re $=$ 100 and $\beta = 100$ in Problem 1, showing the fluid fraction, γ, the flow velocity, **u**, the pressure, p and the temperature, T at iteration steps 8, 30, and 114, respectively. Figure 12 shows the optimization histories of the objective function and the relative complementarity gap. The optimization converged after 114 steps by fulfilling the stopping criterion, where the complementarity gap is less than 10^{-5}. The fluid essentially runs from the inlet to the outlets without dead ends, and a distinct topology can

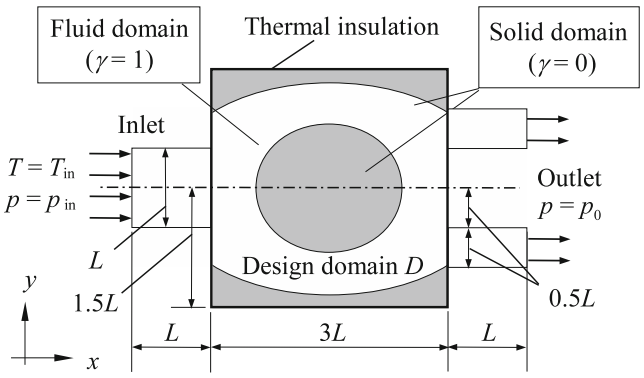

Fig. 10 Problem setting for designing a heat exchanger with one inlet and two outlets

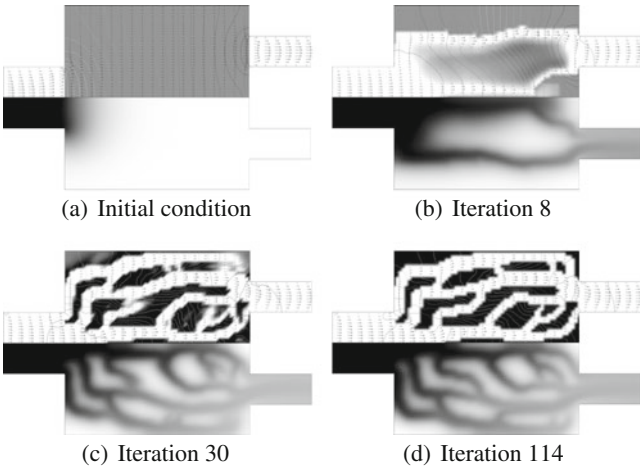

(a) Initial condition (b) Iteration 8 (c) Iteration 30 (d) Iteration 114

Fig. 11 Optimization process of the fluid fraction, γ, with Re $=$ 100 and $\beta = 100$: (*upper half*) gray scale images of the fluid fraction, γ, vector plots of the flow velocity, **u**, and contour lines of the pressure, p; (*lower half*) distributions of the temperature, T

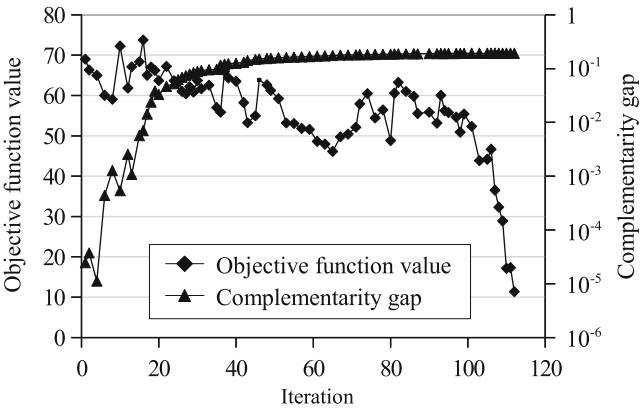

Fig. 12 Optimization histories of the objective function value and the relative complementarity gap for Re $=$ 100 and $\beta = 100$

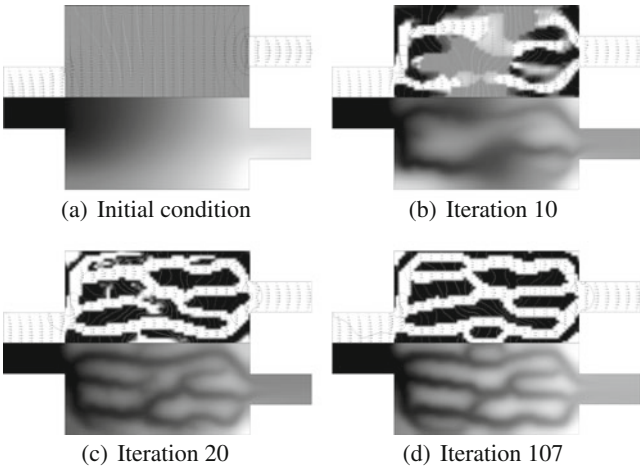

(a) Initial condition (b) Iteration 10 (c) Iteration 20 (d) Iteration 107

Fig. 13 Optimization process of the fluid fraction, γ, with Re $=$ 100 and $V = 0.5$: (*upper half*) gray scale images of the fluid fraction, γ, vector plots of the flow velocity, **u**, and contour lines of the pressure, p; (*lower half*) distributions of the temperature, T

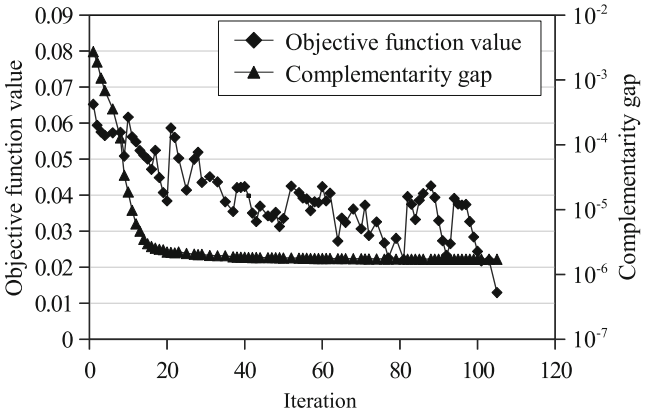

Fig. 14 Optimization histories of the objective function value and the relative complementarity gap for Re $= 100$ and $V = 0.5$

be obtained without gray regions similar to the optimized results of numerical example 1.

Figure 13 provides three snapshots of the optimization process at Re $= 100$ and $V = 0.5$ in Problem 2, showing the fluid fraction, γ, the flow velocity, $\mathbf{u}$, the pressure, p, and the temperature, T, at iteration steps 10, 20, and 107, respectively. Figure 14 shows the optimization histories of the objective function and the relative complementarity gap. The optimization converged after 107 steps by fulfilling the stopping criterion where the complementarity gap is less than 10^{-6}. In the optimized flow channels, there are no dead ends such as those which are found in Dede (2009). One reason for the difference is the formulation of the optimization problem.

6 Conclusions

Based on the density-based approach, we developed a topology optimization method for fluid–thermal interaction problems under a constant input power that is useful for designing heat exchangers with a prescribed amount of input power. For the fluid analysis, based on the work of Borrvall and Petersson, the governing equations for flow in idealized porous media were adopted. In addition to the governing equations, in order to keep the input power constant, we introduced an extra integral equation with respect to the inlet pressure. The inlet pressure was determined by solving the integral equation and was then passed to the boundary condition of the Navier–Stokes equation. For the heat transport analysis, the governing equations were unified into a single equation without separating the solid domain from the fluid domain. The optimization problems were formulated for two types of heat conditions: temperature-dependent and temperature-independent heat sources. Through the numerical examples, we studied that a Reynolds number corresponding to the input power and the heat source parameters, for two types of heat source conditions, were responsible for the topology of the optimized flow channels and their complexity. We also demonstrated the mesh dependency of the topologically optimized results using two differently sized meshes. Finally, in the comparison of the results between one of the optimized results and the corresponding body-fitted model, the errors caused by the expression of the solid region in the flow analysis were seemingly at a tolerable level within the current setting of the numerical simulations. However this has yet to be investigated in more challenging situations with higher Reynolds numbers and a larger ratio of thermal conductivities between the solid and fluid parts.

References

Aage N, Poulsen TH, Gersborg-Hansen A, Sigmund O (2008) Topology optimization of large scale Stokes flow problems. Struct Multidisc Optim 35(2):175–180

Allaire G, Jouve F, Toader AM (2004) Structural optimization using sensitivity analysis and a level-set method. J Comput Phys 194(1):363–393

Azegami H (1994) A solution to domain optimization problems (in Japanese). Trans Jpn Soc Mech Eng 60(A):1479–1486

Azegami H, Takeuchi K (2006) A smoothing method for shape optimization: traction method using the Robin condition. Int J Comput Methods 3(1):21–33

Bendsøe MP (1989) Optimal shape design as a material distribution problem. Struct Optim 1:193–202

Bendsøe MP, Kikuchi N (1988) Generating optimal topologies in structural design using a homogenization method. Comput Methods Appl Mech Eng 71:197–224

Bendsøe MP, Sigmund O (2003) Topology optimization—theory, methods and applications. Springer, New York

Borrvall T, Petersson J (2003) Topology optimization of fluids in Stokes flow. Int J Numer Methods Fluids 41:77–107

Bruns TE (2005) A reevaluation of the SIMP method with filtering and an alternative formulation for solid-void topology optimization. Struct Multidisc Optim 30(6):428–436

Bruns TE (2007) Topology optimization of convection-dominated, steady-state heat transfer problems. Int J Heat Mass Transfer 50(15–16):2859–2873

COMSOL Multiphysics (2008) User's guide, version 3.5a. COMSOL AB

Dede EM (2009) Multiphysics topology optimization of heat transfer and fluid flow systems. In: Proceedings of the COMSOL users conference

Dede EM (2011) Experimental investigation of the thermal performance of a manifold hierarchical microchannel cold plate. In: Proceeding of the ASME 2011, Pacific Rim technical conference and exhibition on packaging and integration of electronic and photonic systems, MEMS and NEMS. doi:10.1115/IPACK2011-52023

Gersborg-Hansen A, Sigmund O, Haber RB (2005) Topology optimization of channel flow problems. Struct Multidisc Optim 30(3):181–192

Gersborg-Hansen A, Bendsøe MP, Sigmund O (2006) Topology optimization of heat conduction problems using the finite volume method. Struct Multidisc Optim 31(4):251–259

Gill PE, Murray W, Saunders MA (2007) User's guide for SNOPT version 7: software for large-scale nonlinear programming. Department of Mathematics, University of California

Iga A, Nishiwaki S, Izui K, Yoshimura M (2009) Topology optimization for thermal conductors considering design-dependent effects, including heat conduction and convection. Int J Heat Mass Transfer 52:2721–2732

Katamine E, Azegami H, Tsubata T, Itoh S (2005) Solution to shape optimization problems of viscous flow fields. Int J Comput Fluid Dyn 19(1):45–51

Kawamoto A, Matsumori T, Yamasaki S, Nomura T, Kondoh T, Nishiwaki S (2011) Heaviside projection based topology optimization by a PDE-filtered scalar function. Struct Multidisc Optim 44(1):19–24

Kondoh T, Matsumori T, Kawamoto A (2012) Drag minimization and lift maximization in laminar flows via topology optimization employing simple objective function expressions based on body force integration. Struct Multidisc Optim 45(5):693–701

Kreissl S, Pingen G, Maute K (2011) Topology optimization for unsteady flow. Int J Numer Methods Eng 87:1229–1253

Li Q, Steven GP, Xie YM, Querin OM (2004) Evolutionary topology optimization for temperature reduction of heat conducting fields. Int J Heat Mass Transfer 47(23):5071–5083

Mohammadi B, Pironneau O (2009) Applied shape optimization for fluids (Numerical mathematics and scientific computation). Oxford University Press, Oxford

Okkels F, Bruus H (2007) Scaling behavior of optimally structured catalytic microfluidic reactors. Phys Rev E 75:016301

Olesen LH, Okkels F, Bruus H (2006) A high-level programming-language implementation of topology optimization applied to steady-state Navier–Stokes flow. Int J Numer Methods Eng 65(7):975–1001

Pingen G, Meyer D (2009) Topology optimization for thermal transport. In: Proceedings of the ASME fluids engineering division summer conference, vol 1, PTS A-C, pp 2237–2243

Pingen G, Evgrafov A, Maute K (2007) Topology optimization of flow domains using the lattice Boltzmann method. Struct Multidisc Optim 34(6):507–524

Pironneau O (1973) On optimal profiles in Stokes flow. J Fluid Mech 59:117–128

Rozvany GIN (2009) A critical review of established methods of structural topology optimization. Struct Multidisc Optim 37(3):217–237

Rozvany G, Zhou M, Birker T (1992) Generalized shape optimization without homogenization. Struct Optim 4:250–252

Wang MY, Wang XM, Guo DM (2003) A level set method for structural topology optimization. Comput Methods Appl Mech Eng 192(1–2):227–246

Yoon GH (2010) Topological design of heat dissipating structure with forced convective heat transfer. J Mech Sci Technol 24(6):1225–1233

Yoon GH (2012) Topological layout design of electro-fluid–thermal-compliant actuator. Comput Methods Appl Mech Eng 209–212(1):28–44